Supplementary Figure 1

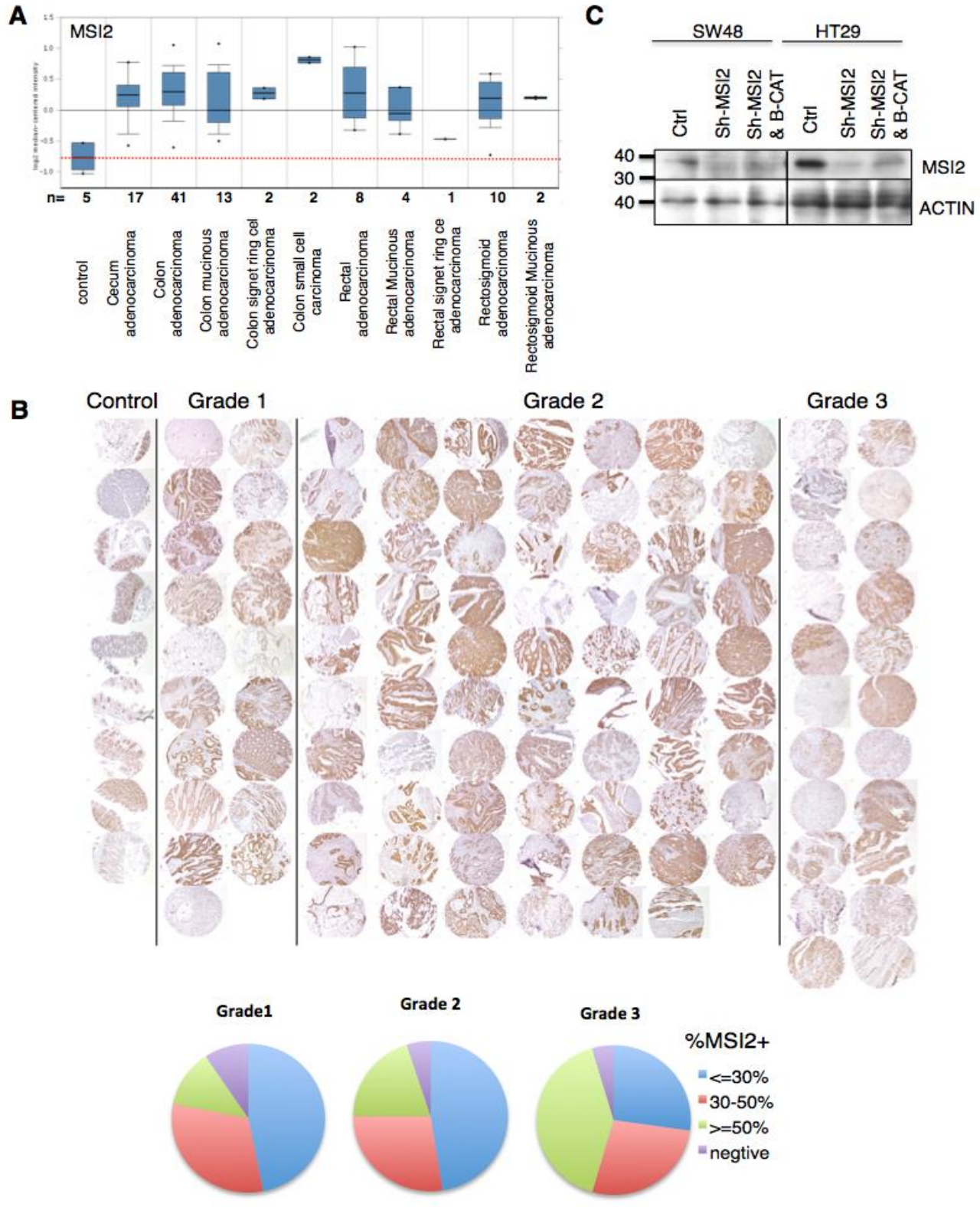

Supplementary Figure 1: MSI2 expression in human colorectal cancers. (**A**) Oncomine transcriptome profiling data showing that MSI2 is overexpressed in a panel of human gastrointestinal cancers. N= the number of distinct patient samples per tumor type, error bars = +/- s.d. from the mean (**B**) Msi2 immunohistochemistry in a graded series of human colorectal adenocarcinomas, with portion of

immunoreactive tissue core quantified below. (**C**) Western blotting confirming MSI2 knockdown in SW48 and HT29 human colorectal cancer cell lines.

Supplementary Figure 2

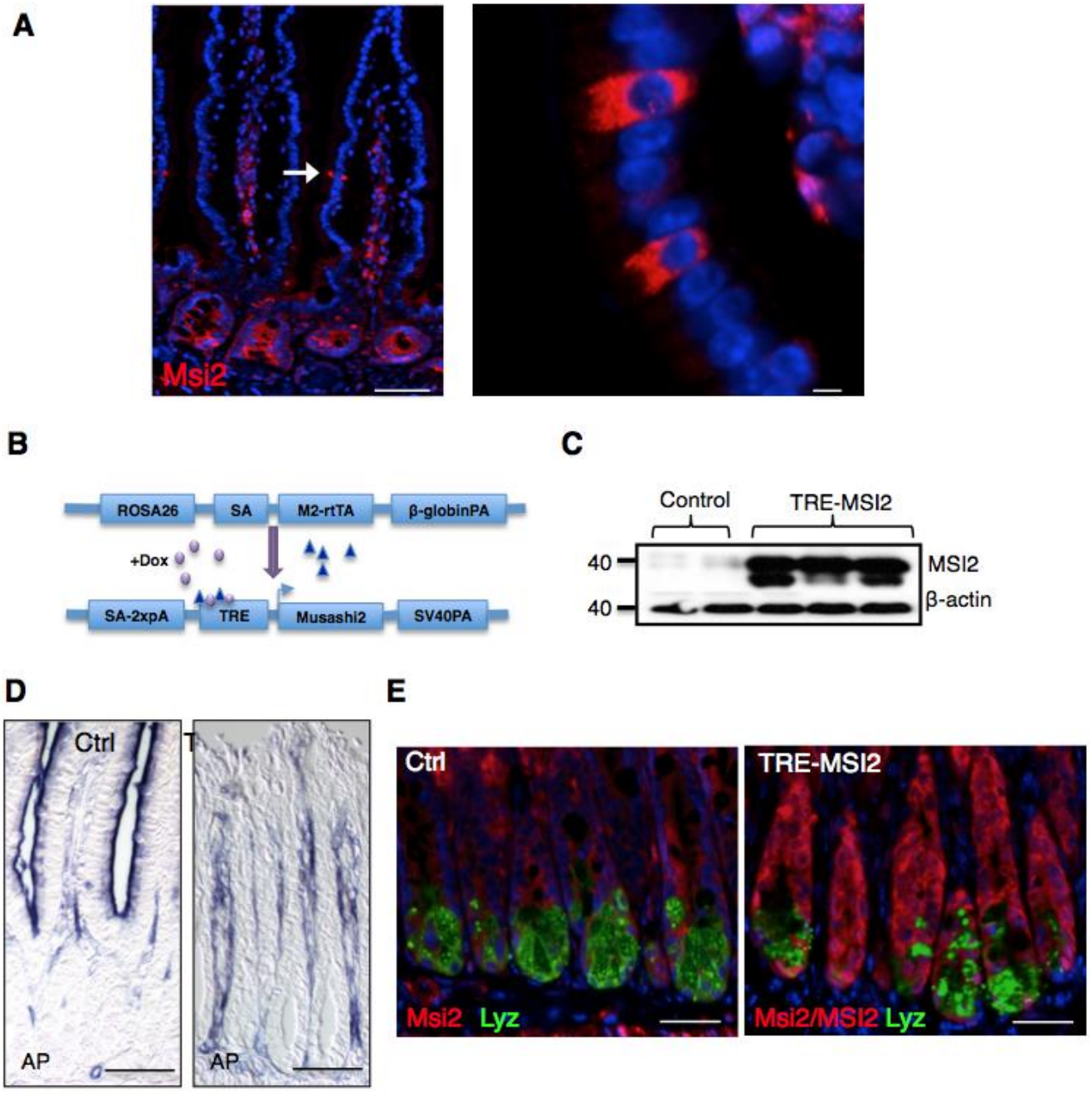

Supplementary Figure 2: Endogenous and inducible MSI2 expression *in vivo*. (**A**) Msi2immunofluorescence staining along the crypt-villus axis showing strong immunoreactivity in the crypts as well as in rare differentiated cells in the villi of wildtype mice (arrows and right panel). Scale bars=50μM (left) and 10μM (right). (**B**) Schematic of doxycycline (Dox)-inducible *MSI2* knockin allele targeted to safe-haven chromatin downstream of the *Col1a1* locus and the modified reverse tetracycline transactivator targeted to and under control of the *ROSA26* locus. (**C**) Western blot demonstrating MSI2 induction upon 24 hours of 2mg/mL Dox administration to the drinking water of Control (*M2rtTA*) or *TRE-MSI2* mice. (**D**) Staining for alkaline phosphatase enzymatic activity (AP) in Control (*M2rtTA*) or *TRE-MSI2* mice. Scale bars=100μM. (**E**) Immunostaining for lysozyme (Lyz, green) and Msi2 (red) in *TRE-MSI2* and control mice 48 hours post-dox induction. Scale bars=50μM.

Supplementary Figure 3

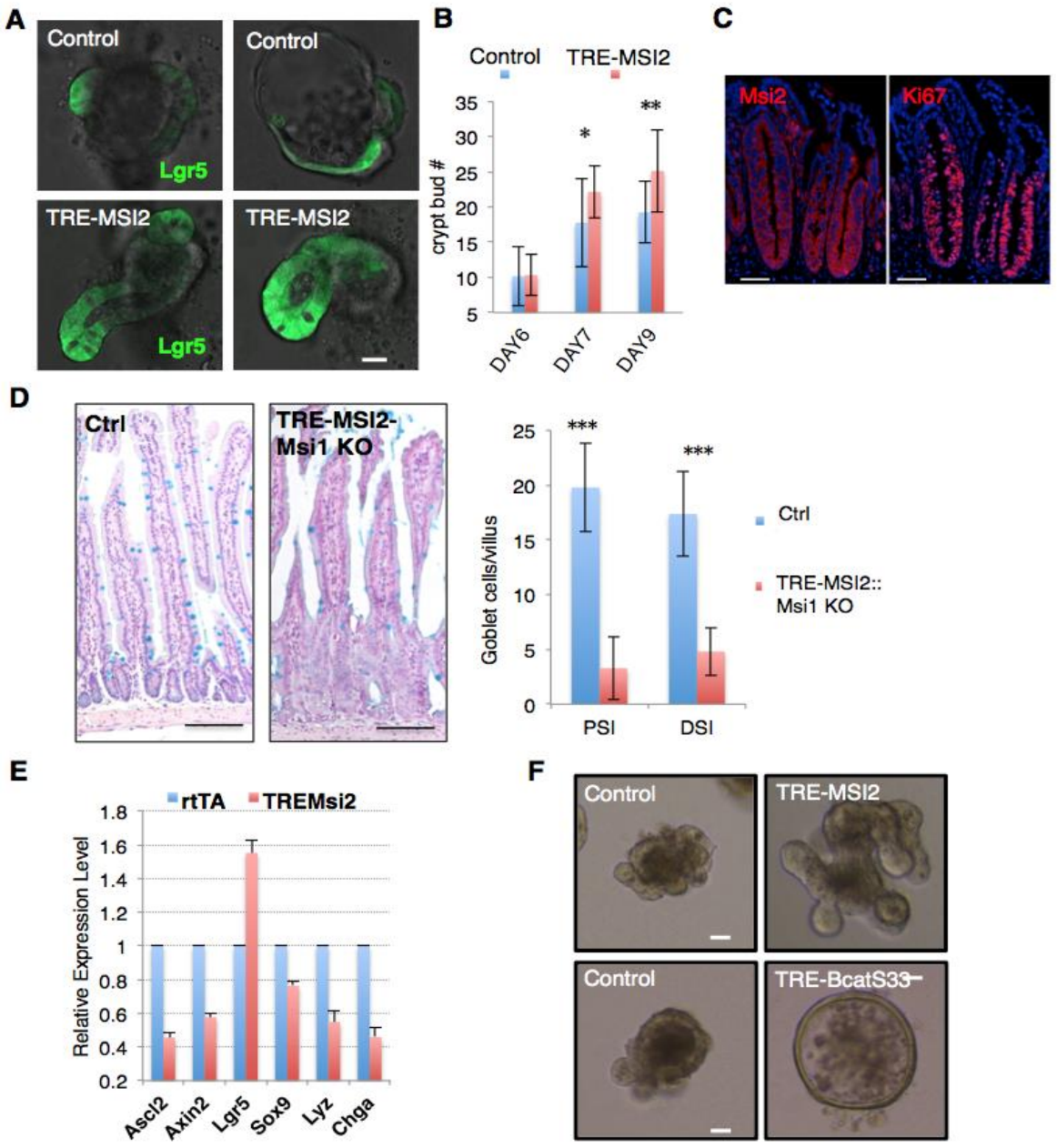

Supplementary Figure 3: *In vivo* and *in vitro* effects of MSI2 induction. (**A**) Representative images of intestinal organoids from *TRE-MSI2::Lgr5-eGFP-IRES-CreER* organoids cultured for 3 days in the presence or absence of 2µg/mL Dox. Scale bars=25µM (**B**) Crypt budding frequency in control (*M2rtTA*) and *TRE-MSI2* organoids at indicated timepoints after seeding and Dox induction. Error bars indicate the s.d. derived from at least 5 organoids per well (n=4 wells) per condition. *:p<0.05, **p<0.005, Student's t-test. (**C**) Immunofluorescence staining for Msi2 and Ki67 in regenerative crypt foci of wildtype mice 3 days after exposure to 12Gy gamma-irradiation. Scale bars=50µM (**D**) Alcian blue staining for goblet cells and quantification of Goblet cell frequency in control *(Msi1$^{flox/flox}$::VillinCreER::M2rtTA)* and *TRE-MSI2-Msi1KO* mice 48 hours after 2mg/mL Dox administration. ***: p<0.0005, Student's t-test. Error bars indicate s.d. derived from at least 20 fields per slide from each of 2 mice per condition. Scale bars=200µM (**E**) QRT-PCR analysis of Wnt-target and differentiation gene expression in 3 wells of control (*M2rtTA*) and *TRE-MSI2* organoids after 2µg/mL Dox induction. (**F**) Representative images of crypt organoids cultured from *TRE-MSI2* or *TRE-β-CatS33* mice followed by 3 days induction with 2µg/mL Dox. Scale bars=10µM.

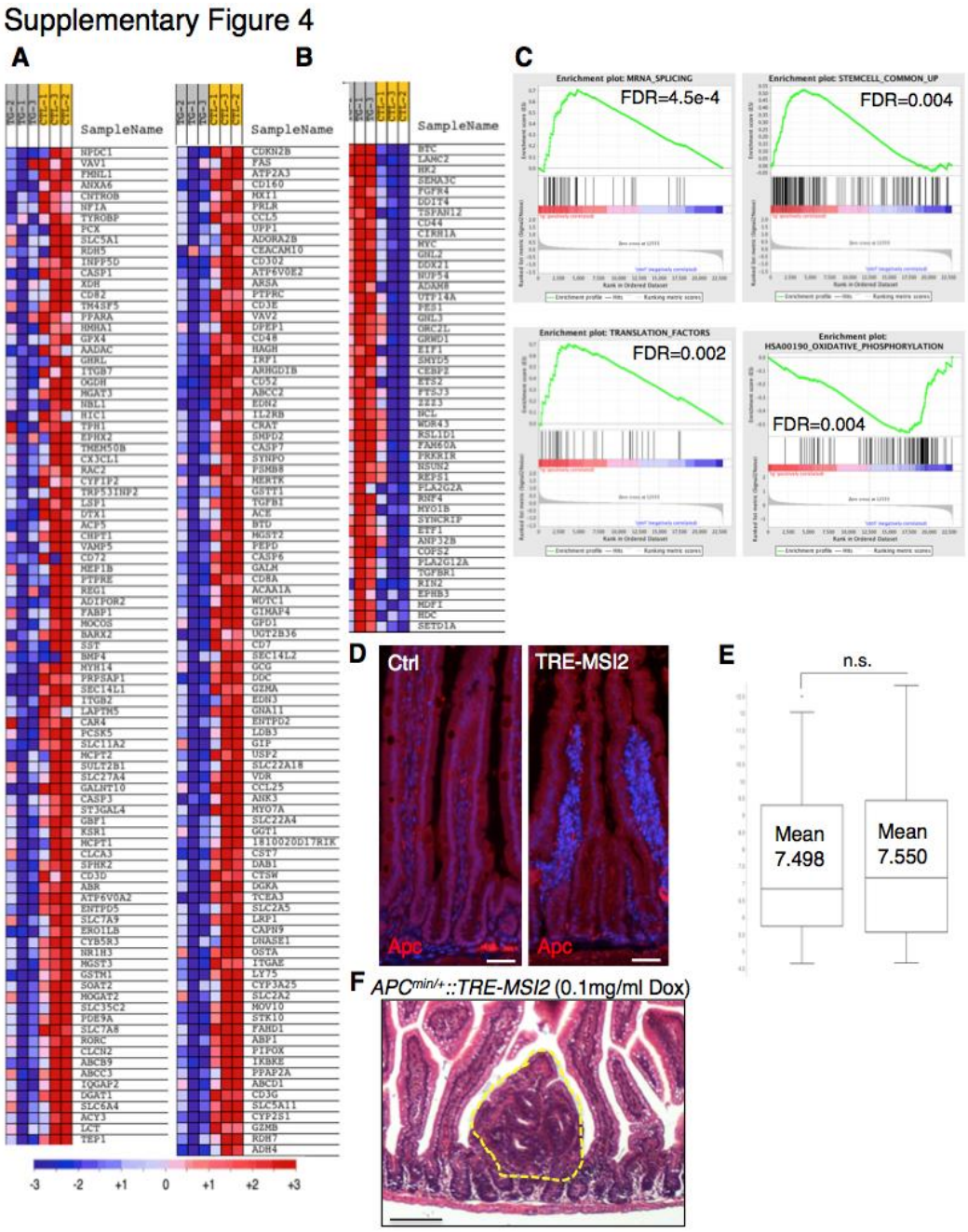

Supplementary Figure 4: Molecular consequences of MSI2 induction. (**A**) Heatmap of genes suppressed by both MSI2 induction and APC loss in the intestinal epithelium (the enriched genes from GSEA plots in **Figure 5B**). Genes in blue are suppressed in *TRE-MSI2* (columns 1-3) compared to controls (column 4-6). (**B**) Heatmap of genes activated by both MSI2 induction and APC loss in the intestinal epithelium (the enriched genes from GSEA plots in **Figure 5B**). Genes in red are activated in *TRE-MSI2* (columns 1-3) compared to controls (column 4-6). (**C**) GSEA plots show a significant enrichment of gene signatures associated with mRNA splicing, translation factors, RAS oncogene signaling, and common stem cell gene signature genes in *TRE-MSI2* vs. control, as well as a negative enrichment (inactivation) of a gene signature associated with oxidative phosphorylation. FDR: False Discovery Rate. (**D**) Immunofluorescence for APC control (*M2rtTA*) and *TRE-MSI2* mice. Scale bars=50μM. (**E**) Box and whisker plots of expression of known direct β-catenin/TCF target genes from control (*M2rtTA*) and *TRE-MSI2* transcriptome profiling analysis. See methods for gene list. (**F**) Representative H&E section of small intestine from *APC$^{min/+}$::TRE-MSI2* mice treated with a low dose of Dox (0.1mg/mL) for three weeks prior to harvest. Normal crypt-villus architecture is observed surrounding an early adenoma formed upon *APC* LOH (dashed yellow outline). Scale bars=200μM.

Supplementary Figure 5

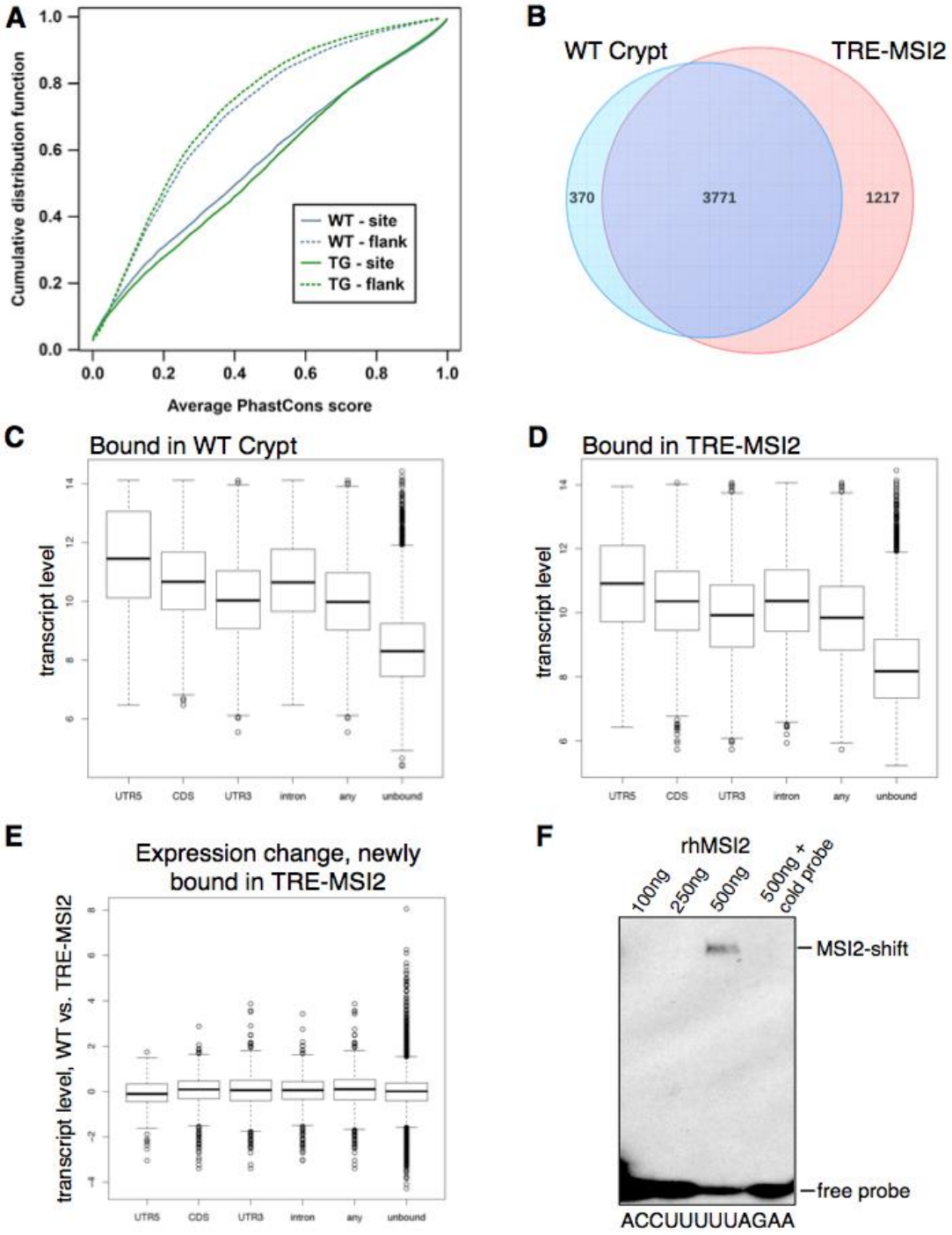

Supplementary Figure 5: *In vivo* MSI2-RNA binding analysis. (**A**) Cumulative distribution of average PhastCons scores in WT Msi2 binding sites (solid blue) versus flanking regions (dashed blue) and TRE-MSI2 binding sites (solid green) versus flanking regions (dashed green). (**B**) Venn diagram showing overlap of transcripts bound in their 3'UTRs only by Msi2 in wildtype intestinal crypts and MSI2 in *TRE-MSI2* intestinal epithelium 24 hours post-Dox induction. (**C, D**) Distribution of absolute abundance of transcripts bound by Msi2 in wildtype crypts in **C** and MSI2 in *TRE-MSI2* intestinal epithelium 24 hours post-Dox induction in **D**. (**E**) Change in expression levels of newly bound transcripts in response to MSI2 induction. (**F**) Electrophoretic mobility shift assays incubating increasing concentrations of recombinant human MSI2 with labeled consensus oligo probe. Unlabeled (cold) probe competes binding of the highest rhMSI2 concentration in the far right lane.

Supplementary Figure 6

A

GO TERM	gene #	P	Benjamini
protein localization	230	7.20E-19	2.90E-15
protein transport	206	7.90E-19	1.60E-15
establishment of protein localization	206	2.00E-18	2.70E-15
intracellular transport	145	1.10E-15	1.10E-12
generation of precursor metabolites and energy	98	4.10E-14	3.30E-11
cellular protein localization	105	6.80E-13	4.50E-10
cellular macromolecule localization	105	1.10E-12	6.20E-10
intracellular protein transport	98	2.00E-12	1.00E-09
nucleotide binding	520	1.60E-15	2.30E-12
small conjugating protein ligase activity	49	3.10E-08	2.30E-05
purine nucleotide binding	416	4.90E-08	2.40E-05
structural constituent of ribosome	54	2.00E-07	7.40E-05
ribonucleotide binding	396	2.90E-07	8.50E-05
purine ribonucleotide binding	396	2.90E-07	8.50E-05
KEGG PATHWAY			
Ribosome	43	1.80E-09	3.30E-07
Adherens junction	38	5.70E-09	5.40E-07
Citrate cycle (TCA cycle)	21	4.20E-08	2.60E-06
Parkinson's disease	51	5.00E-07	2.40E-05
Tight junction	50	2.20E-06	8.10E-05
Wnt signaling pathway	52	9.50E-06	3.00E-04
Oxidative phosphorylation	47	9.70E-06	2.60E-04
Alzheimer's disease	60	1.30E-05	3.10E-04
Huntington's disease	58	6.70E-05	1.40E-03

B

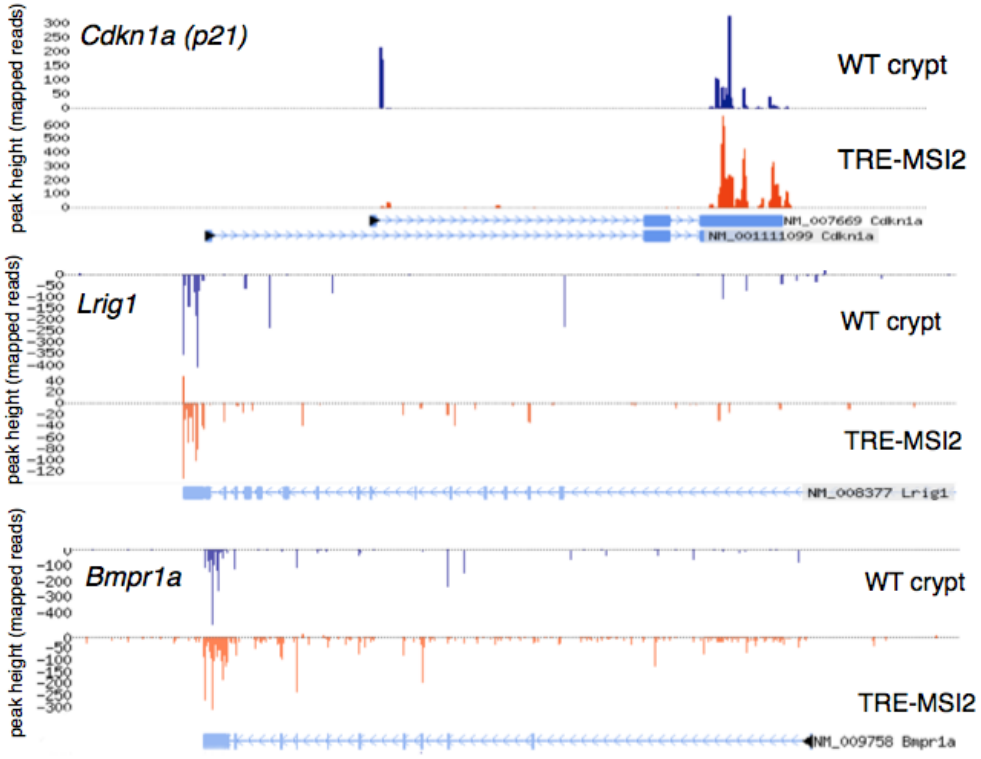

Supplementary Figure 6: MSI2 target transcript pathway analysis. (**A**) Gene Ontogeny (GO) and KEGG pathway analysis of Msi2 CLIP target transcripts. (**B**) CLIP-Seq tracks showing Msi2/MSI2 binding to the 3'UTR of the mRNA encoding the intestinal tumor suppressors p21, Lrig1 and Bmpr1a in wildtype intestinal crypts and in *TRE-MSI2* intestinal epithelium 24 hours post-Dox induction.

Supplementary Figure 7

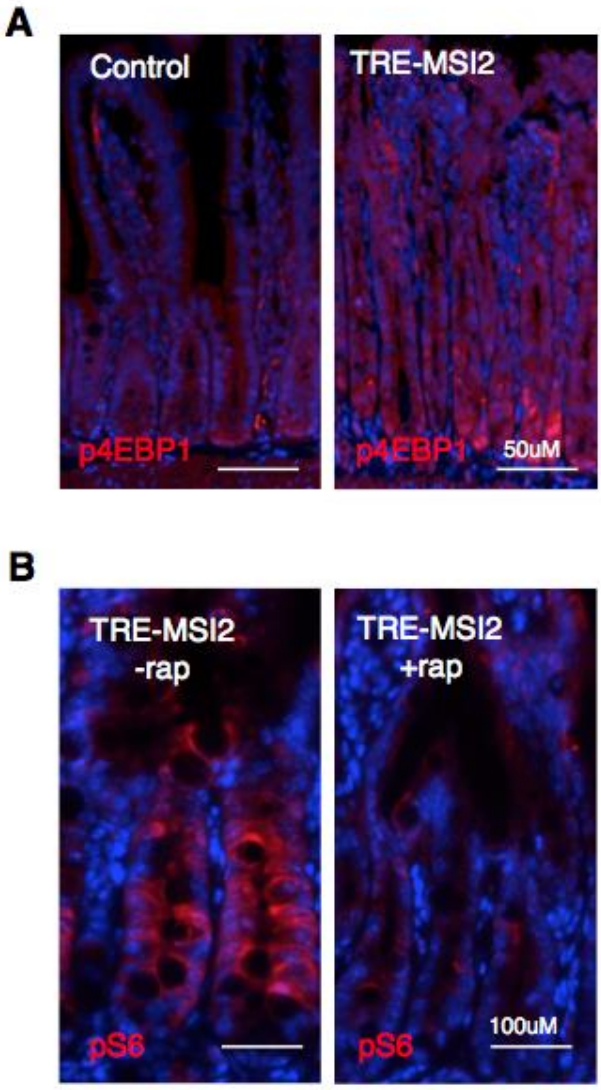

Supplementary Figure 7: MSI2 influence on the mTorc1 pathway. (**A**) Immunofluorescence for p4EBP1 in *M2rtTA* and*TRE-MSI2* mice. Scale bars=50μM. (**B**) Immunofluorescence staining for pS6 in Dox-induced *TRE-MSI2* mice treated with or without Rapamycin. Scale bars=100μM.

Supplementary Figure 8

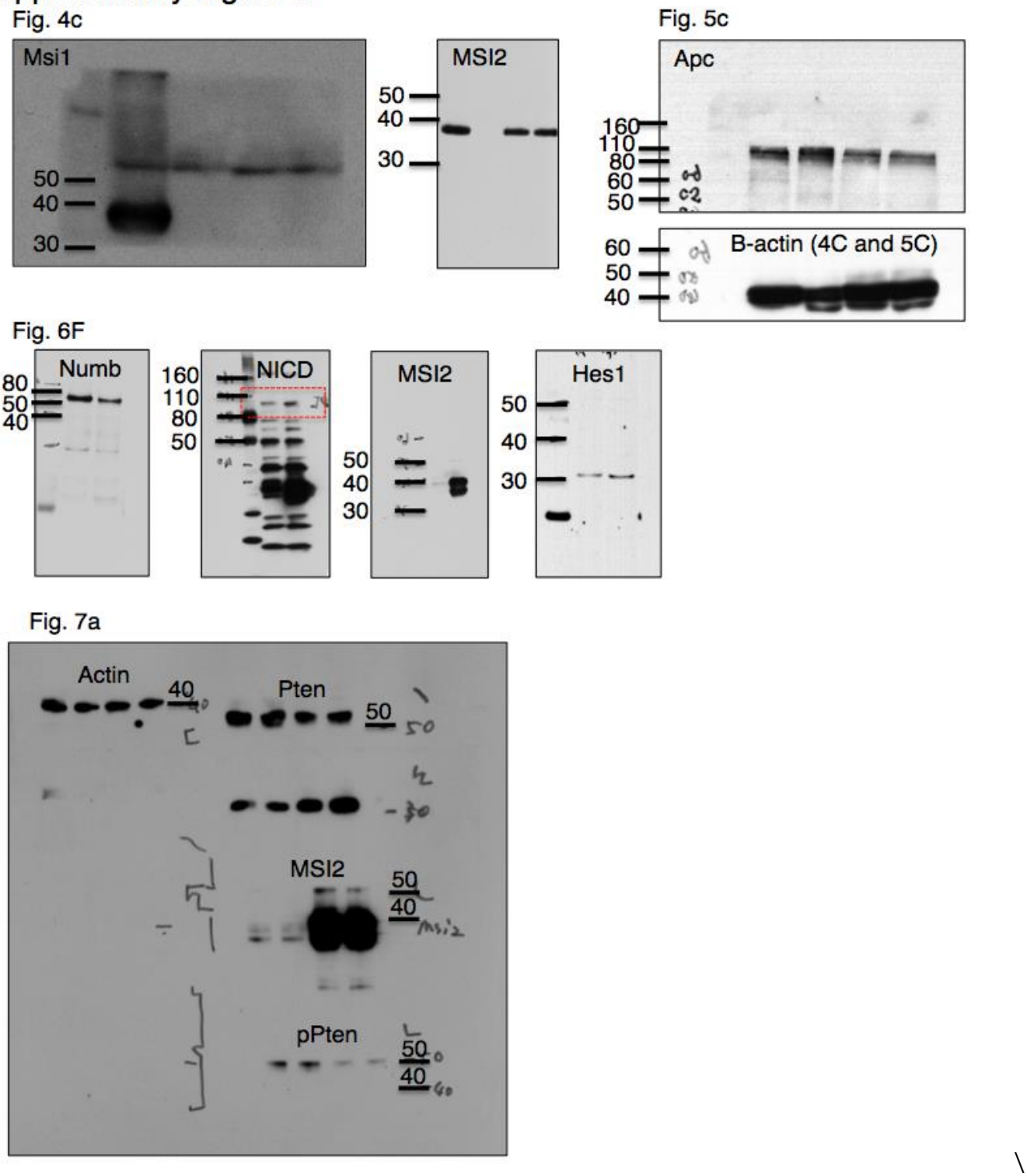

Supplementary Figure 8: Original scans of Western Blots. Scans of autoradiographs of Western Blots appearing in Figures 4C, 5C, 6F, and 7a. Molecular weight markers (kDa) are based on Novex Sharp pre-stained protein standard.